Speckle Interferometry at SOAR in 2016 and 2017

Andrei Tokovinin[1] ⬤, Brian D. Mason[2], William I. Hartkopf[2] ⬤, Rene A. Mendez[3], and Elliott P. Horch[4,5] ⬤
[1] Cerro Tololo Inter-American Observatory, Casilla 603, La Serena, Chile; atokovinin@ctio.noao.edu
[2] U.S. Naval Observatory, 3450 Massachusetts Avenue, Washington, DC, USA; brian.d.mason@navy.mil
[3] Universidad de Chile, Casilla 36-D, Santiago, Chile; rmendez@u.uchile.cl
[4] Department of Physics, Southern Connecticut State University, 501 Crescent Street, New Haven, CT 06515, USA; horche2@southernct.edu

Abstract

The results of speckle interferometric observations at the 4.1 m Southern Astrophysical Research Telescope in 2016 and 2017 are given, totaling 2483 measurements of 1570 resolved pairs and 609 non-resolutions. We describe briefly recent changes in the instrument and observing method and quantify the accuracy of the pixel scale and position angle calibration. Comments are given on 44 pairs resolved here for the first time. The orbital motion of the newly resolved subsystem BU 83 Aa,Ab roughly agrees with its 36-year astrometric orbit proposed by J. Dommanget. Most *Tycho* binaries examined here turned out to be spurious.

Key words: binaries: visual

Supporting material: machine-readable tables

1. Introduction

We report here a large set of double-star measurements made at the 4.1 m Southern Astrophysical Research Telescope (SOAR) with the speckle camera, HRCam. This paper continues the series published by Tokovinin et al. (2010a, 2010b, hereafter TMH10, 2014, 2015, hereafter SOAR14, 2016b), Hartkopf et al. (2012), and Tokovinin (2012).

The objects were selected mostly among nearby (within 200 pc) binaries resolved by *Hipparcos*, continuing our previous effort in this direction that mirrors the effort in recent years at WIYN (Horch et al. 2017) and DCT (Horch et al. 2015) telescopes on the analogous Northern *Hipparcos* sample. Similar to the Northern program, the main goal is to identify and follow *Hipparcos* binaries that show relatively fast orbital motion and that would be good candidates for mass determinations in the coming years. It is especially important to obtain orbital data on these systems in advance of final *Gaia* results, so that the full power of the *Gaia* parallaxes can be brought to bear on the determination of the mass sum. We also followed the fast orbital motion of close pairs and subsystems discovered previously at SOAR or elsewhere, with the aim of characterizing their orbits. These data are actively used for orbit calculation (Gomez et al. 2016; Mendez et al. 2017; Tokovinin 2016, 2017, 2018b, 2018c; Mason et al. 2018). To provide additional bright targets when observing conditions are mediocre or poor, we observed as a "filler" potentially interesting neglected pairs suggested by R. Gould (2018, private communication) and binaries with known orbits.

2. Observations

2.1. Instrument

The observations reported here were obtained with the high-resolution camera (HRCam)—a fast imager designed to work at the 4.1 m SOAR telescope (Tokovinin & Cantarutti 2008; Tokovinin 2018a). For practical reasons, the camera was mounted on the SOAR Adaptive Module (SAM, Tokovinin et al. 2016a).

However, the laser guide star of SAM was not used (except in 2016 January) because it was not needed and, moreover, reduced the productivity by adding an overhead. The deformable mirror of SAM was passively flattened and the images are seeing-limited. The SAM module contains the atmospheric dispersion corrector (ADC) and helps to calibrate the pixel scale and orientation of HRCam (see SOAR14). The transmission curves of HRCam filters are given in the instrument manual.[6] We used mostly the Strömgren *y* filter (543/22 nm) and the near-infrared *I* filter (788/132 nm).

In 2016 May, at the end of the run, the Luca-DL detector of the HRCam failed after 10 years of faithful service and one repair by the vendor (Andor) during this period. In 2016 December, we used the Luca-R camera loaned by the STELES instrument team. With a 75 mm camera lens, the pixel scale was 14.30 mas. A similar Luca-R camera was also used in 2014, as described in SOAR14. However, that frame-transfer CCD had imperfect charge transfer in the column direction, leading to a partial loss of resolution. This time, the loaned Luca-R camera was characterized in this respect, and we found that it presents a similar problem, although to a smaller extent. A typical charge spread along the columns was found to be from 2 to 3 pixels. We did not account for this effect in the data processing (Section 2.4), as in 2014 (Tokovinin et al. 2015), but in some cases could reduce its influence by using a reference spectrum with a comparable smear. One consequence of this problem is the reduced resolution in the vertical (usually north–south) direction for the fainter targets.

Meanwhile, Dr. N. Law from the University of North Carolina has kindly loaned us a better electron multiplication (EM) CCD camera, iXon X3 888 (hereafter iXon-888), also manufactured by Andor.[7] Unlike Luca, this is a back-illuminated EM CCD with a substantially higher quantum efficiency (QE) and a deeper cooling. The detector has 1024^2 pixels. Sending this export-controlled camera to Chile took longer than expected, so it could be used only in 2017. The
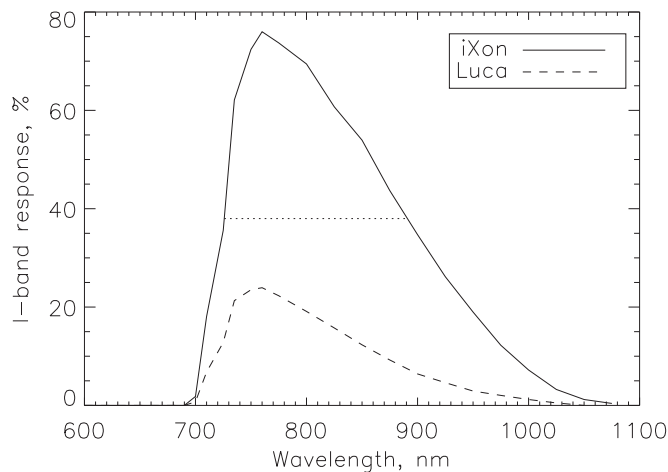

Figure 1. Product of the *I*-filter transmission curve and the detector quantum efficiency. The dotted horizontal line shows the FWHM for the iXon camera.

larger 13-micron pixel size required a change of the re-imaging lens in HRCam to one with 125 mm focal length, resulting in a pixel scale of 15.75 mas. The mechanical structure was reinforced to hold this heavier camera. The HRCam PC computer was also replaced. As the cable connecting the camera to the computer is short, the PC was located close to the HRCam. The data acquisition software was adapted to the new detector by R. Cantarutti. The minimum exposure time for the standard 200×200 pixel region was 24 ms, and this exposure time was used mostly throughout 2017. With this exposure time, the 50 Hz vibrations, when present, affect both resolution and sensitivity of HRCam (Tokovinin et al. 2010a; Tokovinin 2018a). A shorter exposure of 6.7 mas is possible in the so-called cropped sensor mode. This mode was tested at the telescope, but not used because switching between readout modes cannot be done rapidly.

Figure 1 shows the QE of the detector multiplied by the transmission of the filter *I*. This filter cuts off only short wavelengths, so the bandwidth depends on the detector response. The curve for iXon-888 has an FWHM of 170 nm (from 725 to 895 nm), with an effective wavelength of 824 nm. With this wide bandwidth, the effective wavelength depends on the source color; it is substantially longer for red stars. For comparison, the corresponding QE curve of the Luca-DL camera with the same filter is also plotted; it has a central wavelength of 788 nm and a narrower FWHM bandwidth of 132 nm.

2.2. Observing Procedure

In speckle interferometry, the data accumulation takes only a short time (typically 8 s). Therefore, the observing efficiency is mainly determined by the telescope slew and setup (centering of the star, setting the ADC, and changing filters). The standard procedure at SOAR requires the operator to select target coordinates from a list and to command the slew to the new position. When the observing list contains several hundred targets, this is a labor-intensive task.

To address this problem, we developed in 2014 a speckle observing tool, written in IDL. In preparation for the run, targets are selected from the database including all observed objects; it contains the equatorial coordinates, proper motions, magnitudes, separations, date of the last observation at SOAR, and comments. The selected information is used by the

observing tool with a graphic user interface. It displays an area of the sky around the selected target in the horizontal (azimuth and elevation) coordinates. The next target is selected by clicking on the display or entering its number. All previous observations of the selected object at SOAR can be listed on the screen, if desired. By pressing a button, the target coordinates for the current moment (accounting for the proper motion) are sent to the SOAR telescope control system (TCS). The new SOAR TCS moves the telescope if the requested slew is less than $5°$ (recently extended to $15°$), otherwise confirmation of slew by the telescope operator is needed. This tool greatly reduces the load on the telescope operators. At the same time, the target name is sent to the instrument software, hence there is no need to type it. The observer only has to center the target and to select the filter and the detector parameters. Use of this observing tool has improved the efficiency to the point where 300 targets could be observed in one winter night.

The choice of the next target remains manual, considering priorities and variable observing conditions. For example, useful measures of bright stars can be made through transparent clouds or under very poor seeing. So, the observing program contains extra "filler" targets for such situations. The observing tool also helps to optimize telescope slews. The combination of priorities, diverse observing conditions, slew, and visibility constraints defines which program stars are actually observed in each run. In 2017, most observations were made remotely from La Serena. This is very convenient, especially for short observing runs.

2.3. Observing Runs

The observing time for this program was allocated through NOAO (2.5 nights in 2016, programs 16A-0005 and 16B-0044, PI A.T.) and by the Chilean National Time Allocation Committee, CNTAC (4 nights in 2016A, program CN2016AB-4, PI R.A.M.). Some data reported here (e.g., on calibration binaries) were also collected during observations with HRCam for other programs (2.5 nights in 2015B, 15B-0268, PI C. Briceño, 1 night in 2016A/B, PI B. Pantoja, and 2 nights in 2016A, PI Ji Wang, Kepler-2 follow-up). Measures and discoveries resulting from the Kepler-2 (*K2*) program are included in this paper. In 2017, 2 nights per semester were assigned through NOAO for multiple-star observations (PI A.T., programs 17A-0008 and 17B-0066). All observations were made by A.T., sharing the allocated time between programs to cover the whole sky and to improve temporal cadence for pairs with fast orbital motion.

Table 1 lists the observing runs, the calibration parameters (position angle offset θ_0 and pixel scale in mas), and the number of objects observed for all programs covered in each run. Its last column gives the median FWHM of the recentered images, β, determined during data processing.

Run 1 (2.5 nights in 2016 January) was dedicated to observations of young stars (PI C. Briceño) in Orion and Chamaeleon, see Briceño & Tokovinin (2017). The image quality (hence sensitivity) was improved using the UV laser, allowing us to observe stars of $I \sim 13$ mag with exposure times of 0.1 or 0.2 s (not quite at the diffraction limit, however, with a median FWHM of $0.''33$). When the main targets were not visible, double stars were observed without laser in the standard speckle mode. The seeing was good during most of this run.

Table 1
Observing Runs

Run	Dates	θ_0 (deg)	Pixel (mas)	N_{obj}	β ('')
1	2016 Jan 16–18	−3.00	15.23	270	0.77
2	2016 Feb 18–20	−2.72	15.23	474	0.83
3	2016 May 20–23	0.20	15.23	315	1.15
4	2016 Dec 12	−12.0	14.30	41	0.64
5	2016 Dec 15–17	0.30	14.30	493	0.67
6	2017 Apr 13	−0.1	15.75	152	0.82
7	2017 May 15	−0.1	15.75	201	0.80
8	2017 Jun 6	−0.1	15.75	319	0.68
9	2017 Jul 14	−0.1	15.75	161	0.88
10	2017 Aug 7	0.1	15.75	116	1.02
11	2017 Sep 5	0.0	15.75	275	0.73
12	2017 Oct 4	−0.15	15.75	41	0.90
13	2017 Oct 28	0.2	15.75	122	0.55

Run 2 (2.5 nights in 2016 February) was split between observations of multiple stars (0.5 nights), *Hipparcos* binaries (2 nights), and the program of B. Pantoja (0.5 night). It enjoyed clear skies and slow wind speed, with average seeing. On the last night of the run, the phenomenon of optical ghosts was observed, as described below in Section 2.6.

Run 3 (4 nights in 2016 May) suffered from poor weather and technical problems. The first night started with a strong wind and a high humidity of 83%. The seeing was extremely poor (2''–3''). The telescope was closed for high humidity most of the night, so only 44 bright stars could be observed. The following night was clear, with a strong wind, poor seeing, and occasional passage of transparent clouds. The third night was lost to clouds. When some bright stars were observed between the clouds, frequent failures of the Luca-DL camera prevented operation. On the last night of the run (also mostly cloudy) we replaced the camera, but these data are discarded here, being insufficient in both quality and quantity for a meaningful analysis. The first two nights of this run were assigned to the Kepler-2 (*K2*) follow-up, which is the Yale program managed by Ji Wang (at the California Institute of Technology, Caltech). He provided the list of targets, including all known binaries from the Washington Double Star Catalog, WDS (Mason et al. 2001) in the *K2* fields (R.A. range from 16 to 20 hr, decl. from −31° to −25°). Pairs wider than 4'' could not be measured with HRCam; however, we discovered 10 new components in known binaries (see Section 3.3). The 2 last nights (May 22 and 23) were assigned to the program of R. Mendez (CNTAC) on *Hipparcos* binaries. In this run, the new SOAR TCS was operational, allowing small slews to be commanded directly by the speckle observing tool.

Run 5 (2.5 nights in 2016 December) was preceded by 2 hours of engineering observations on December 12, treated here as a separate run 4. As described in Section 2.1, we used the loaned Luca-R camera in these runs. The sky was clear, and the seeing was average.

Run 6 in 2017 April used for the first time the new iXon-888 CCD camera, on an engineering night with a strong wind and occasional transparent clouds.

Run 7 in 2017 May used 1 allocated night. For several hours, the telescope remained closed owing to high humidity.

Run 8 on 2017 June 6 used 1 full night allocated for the multiple-star program. The sky was mostly clear. A record number of 319 targets were observed during this night.

Run 9 in 2017 July was a half-night allocation for the program by B. Pantoja. Some observations were made through transparent clouds.

Run 10 used the engineering time on a partially cloudy night, when other planned tasks could not be accomplished.

Run 11 was almost a full night of 2017 September 5 (engineering). The regular allocated night of September 11 was lost to clouds.

Run 12 on 2017 October 4 used only 2 hr of engineering time, again observing through the clouds.

Run 13 on 2017 October 28 (half-night) enjoyed a clear sky and good seeing. The increased sensitivity of the new camera allowed us to observe some stars as faint as $I = 14$ mag without adaptive correction. However, SOAR vibrations affected some data of this run.

2.4. Data Processing

Data processing is described in TMH10 and subsequent papers of this series. We recall it here briefly, emphasizing the caveats. A series of short-exposure images are recorded as FITS cubes, typically of $200 \times 200 \times 400$ pixel size, two cubes per target and per filter. A larger image size of 400×400 pixels is used for pairs wider than 1''5. The power spectrum (PS) of each data cube is computed after subtracting the bias and applying a threshold to eliminate noise in empty pixels. In the case of iXon-888 cooled to −60°C, the dark current is negligible, while the bias has a gradient in the vertical direction only; the software was adapted accordingly. Along with the PS, the program computes the average recentered image and the shift-and-add (SAA) image centered on the brightest pixel. The auto-correlation function (ACF) is computed later from the PS, filtered to remove low spatial frequencies.

Binary companions are detected in the ACF. Their parameters (position angle θ, separation ρ, and magnitude difference Δm) and their formal errors are determined by fitting a model to the high-frequency part of the PS; the model is a product of the reference PS and the PS of two point sources. In most cases, the reference is derived from the azimuthally averaged PS of the object itself (TMH10). Vibrations, telescope wind shake, and residual aberrations such as astigmatism create two-dimensional patterns in the PS that are not captured by the model. Using another observed object (either unresolved or with a substantial magnitude difference) helps here, as explained in Tokovinin et al. (2016b). However, the PS structure constantly evolves in time, complicating its modeling.

Measurements of binaries wider than $\sim$0''1 are not sensitive to the PS model and are very robust. In contrast, for close pairs with a substantial magnitude difference (Δm), the results of the fitting procedure do depend on the PS structure, the use (or not) of the real on-sky reference, and its conformity to the actual PS. Some measures presented here are affected by these poorly quantified biases. Differences between positions measured in the y and I filters are indicative of such cases. Measures of binaries at or below the diffraction limit (27 mas in the y filter and 40 mas in the I filter) should also be treated with caution. Less reliable measurements are marked by colons.

Yet another caveat is related to the differential photometry of binaries wider than $\sim$1''. The speckle signal is reduced by anisoplanatism, biasing the derived Δm to higher values. If the pair is resolved in the centered images, an alternative photometric procedure corrects for this bias (see TMH10).

The resolution in the centered images, β, is also determined in the process. However, images of wide pairs can be partially truncated, especially when the wind-induced telescope shake causes substantial image wander or when the seeing is particularly poor. Such situations also lead to an overestimate of Δm. It is safe to consider the published Δm of wide pairs as upper limits. The photometry is reliable when there are several mutually agreeing measurements of Δm.

Speckle processing determines the PA of the pair modulo 180°. When the companion is seen in the SAA images, the correct quadrant can be chosen, provided that $\Delta m > 0.3$ mag; otherwise, the two peaks in the SAA image are equal and the strongest one cannot be identified. Quadrants defined in this way are marked by the flag "q" in the data tables. The flag "*" indicates binaries resolved in the centered images, where the quadrants are also known.

2.5. Calibration of Position Angle and Scale

The calibration of the PA and pixel scale was done with respect to 64 wide pairs, as explained in SOAR14. It was revisited and improved here by including more calibrators and the latest data. Moreover, the motion of some calibrators is now modeled by orbits adjusted to fit the SOAR data, rather than by linear functions of time. A few stars showing obvious deviations from the models were removed from the list of calibrators. One such ex-calibrator that turned out to be a triple system is presented below in Section 3.4. A typical rms deviation of the calibrator binaries from the models is from 1 to 3 mas in both radial and tangential directions. Overall, measures of the calibrators comprise about 10% of all measures presented here.

In run 3, the new SOAR TCS was used for the first time. We found that the instrument PA, nominally set at 0°, 90°, or some other round number, was incorrect in a small number of cases, causing manifestly wrong angle measurements. This prompted us to recompute all instrument PAs using the information on the telescope elevation, Nasmyth rotator angle, and star position. The recomputed angles differed from their nominal round values; they were used in the data reduction. With the recomputed instrument angles, the rms scatter in the PA of the calibration binaries decreased from 0°7 to 0°4, indicating the appropriateness of this correction. However, the remaining scatter is still substantially larger than normal. It is possible that the mechanical rotation of the Nasmyth bearing had failures preventing it from reaching the required angle. This problem apparently persisted in run 5, but the PAs were not recomputed because this did not reduce the scatter of the calibrators, 0°4. The small engineering run 4 suffered from the communication problem between the instrument software and the TCS; some PAs in these data might be erroneous. In contrast, the calibrator observations in 2017 show a small PA scatter from 0°1 to 0°2 in all runs.

Figure 2 plots the residual deviations of the calibrators in PA versus time. The distribution of points in time corresponds to the observing runs in Table 1. Despite the correction of the instrument angles in run 4, there is one deviant measure. Run 5 also shows a larger than usual scatter in the PA residuals of the calibrators. When all 231 observations of the calibrators during two years are treated as one data set, the rms scatter in PA is 0°25. The global rms scatter of the scale factor is 0.0041.

Four binaries (WDS J04136+0743, J07277+2127, J09285 +0903, and J22409+1433) have very accurate orbits based on
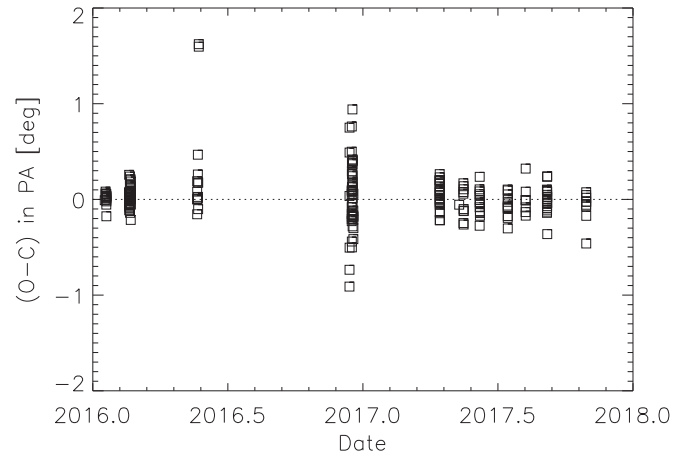

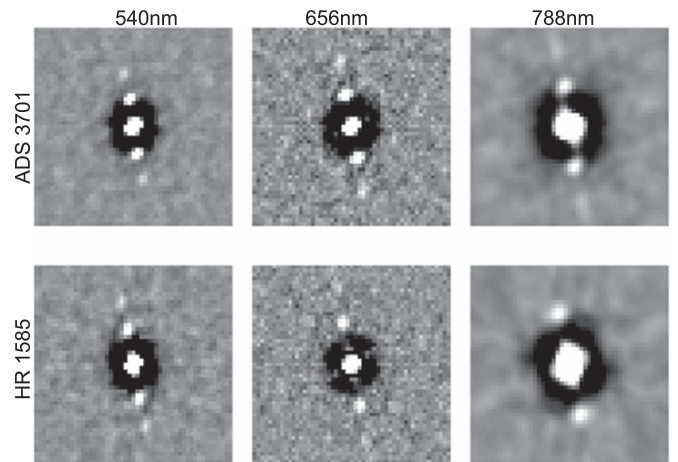**Figure 2.** Residual in position angle of the calibration stars, plotted vs. time.

Figure 3. ACFs of ADS 3701 (top row) and HR 1585 (bottom row) in three filters showing OGs. Fragments of ACFs of 51 × 51 pixels (0″78) recorded on 2016 February 20 are shown. North is up, east to the right; the intensity scale is arbitrary.

long-baseline interferometry (Muterspaugh et al. 2010a, 2010b). A total of 10 measures of these binaries have mean residual in PA of −0°15 with rms scatter of 0°28. The mean residual in separation is 3.3 mas with the rms of 2.0 mas. This comparison is the external check of the data accuracy. The majority of visual orbits are less accurate than our measures.

2.6. Optical Ghosts

During the first hours of the night on 2016 February 20, the phenomenon of optical ghosts (OG) was observed. The sky was clear, the wind speed was low or zero. We pointed and unexpectedly resolved ADS 3701, a known "ghost" binary (Tokovinin 2012). However, the bright star HR 1585 observed immediately after also displayed a similar doubling. Both bright objects were observed with short 2 ms exposures, eliminating a potential effect of telescope vibration. Figure 3 shows the speckle ACFs of these two objects in three filters. Unlike real double stars, the separation of the "companions" increases in proportion to the wavelength. Moreover, we see the second, fainter companions with double separation. The phenomenon is obviously associated with diffraction on a periodic structure where the first and second diffraction orders are seen. The separation of the first-order diffraction maximum

Table 2
Examples of Optical Ghosts

Date (UT)	Filt.	WDS α,δ(2000)	ROT (°)	AZ (°)	EL (°)	ROT−EL (°)	θ (°)	ρ (″)
2016 Feb 20 00:18	I	04357+0127	77.3	334.6	55.3	22.0	161.7	0.178
2016 Feb 20 09:26	I	14375+0217	58.8	358.4	57.3	1.5	167.6	0.231
2016 Feb 20 09:26	y	14375+0217	58.8	358.4	57.3	1.5	166.2	0.153
2016 Feb 21 01:12	y	05348+0929	65.9	339.6	47.9	18.1	167.5	0.155
2016 Feb 21 01:14	Hα	05348+0929	65.9	339.6	47.9	18.1	167.0	0.184
2016 Feb 21 01:16	y	05079+0830	73.0	328.8	45.9	27.1	164.9	0.092
2016 Feb 21 01:30	y	05354−0555	93.0	321.4	60.0	33.1	164.9	0.187

Note. The columns contain ROT—Nasmyth rotator angle; AZ —telescope azimuth; EL—telescope elevation; ROT−EL—instrument angle on the sky; θ and ρ—PA and separation of the OG processed as a binary companion.

$\rho \sim 0\rlap{.}''1$ is related to the grating period $b = \lambda/\rho$, with b calculated to be from 0.8 to 1.1 m.

The OGs were observed in three objects that were located close to each other on the sky, then disappeared in the following group of objects in the same sky area, and reappeared again in two more episodes, each counting several successive objects. The three OG episodes occurred during a time period of about one hour (from UT 0:46 to 1:37), and no more OGs were seen for the rest of the night. Data examination revealed that similar OGs occurred on the previous night around UT 0:18 and 9:26. The wind speed on the previous night was also very low.

Table 2 provides the circumstances of some OG observations that might help in finding their origin. The first three columns give the UT date of the observation, filter, and WDS designation of the target. The WDS is used only for convenience, as OGs are unrelated to binary companions (in fact, 04357+0127 is the single star HIP 21411). Then follow the angle of the Nasmyth rotator ROT, the telescope azimuth AZ, and the elevation EL. The difference EL−ROT shows the instrument angle relative to the telescope primary mirror or, equivalently, the parallactic angle. The last two columns give the position angle θ and the separation ρ of the OGs measured as if they were double stars.

The position angles of OGs observed on both nights are confined within a narrow range, close to but not exactly aligned with the north–south direction. The parallactic angle ranged over 32°, so OGs are not aligned in the vertical direction. The OGs were observed when the telescope was pointing to the north–north–east, at moderate elevation. They appeared and disappeared on a timescale of several minutes; however, in the pair of data cubes of the same star taken one after another, the OGs are always similar.

The nature of OGs is mysterious. We could reproduce the OGs in simulated speckle images by placing in the beam a fixed periodic phase screen, in addition to the random atmospheric perturbation corresponding to the $0\rlap{.}''7$ seeing. By trial and error, we found that the clipped sine wave (only positive half-periods, zero otherwise) with a spatial period b of 1 m and a path-length amplitude of 0.2 μm matches the OGs seen in various filters, creating two diffraction orders of approximately correct relative intensity.

The origin of such quasi-periodic phase disturbances is not known. They are certainly not related to the instrument or telescope, as evidenced by the position angles. The fact that OGs appear only episodically under zero-wind conditions suggests that they might be a transient atmospheric phenomenon like stratification or waves. Systematic wavefront distortion under low wind has been observed at the Very Large Telescope (VLT) by Sauvage et al. (2015). OGs corresponding to the grating period of ∼2 m were seen during previous speckle runs at SOAR (see Figure 11 in TMH10). However, OGs with two diffraction orders and a larger separation were observed at SOAR for the first time only now. The OG phenomenon can explain some false double-star discoveries made with speckle interferometry in the past. We mistakenly assumed HIP 75050 to be a newly resolved pair before realizing that its measure refers to the OG.

3. Results

3.1. Data Tables

We do not report here the results belonging to other PIs, namely the Orion and Chamaeleon (Briceño & Tokovinin 2017) surveys and the targets observed for B. Pantoja. However, observations of binaries in the *K2* fields (PI Ji Wang) are published here with the PI's permission.

The data tables have the same format as in the previous papers of this series. They are available in full only electronically. Table 3 lists 2483 measures of 1570 resolved pairs and subsystems, including 44 newly resolved pairs. The columns of Table 3 contain (1) the WDS (Mason et al. 2001) designation, (2) the "discoverer designation" as adopted in WDS, (3) an alternative name, mostly from the *Hipparcos* catalog, (4) Julian year of observation, (5) filter, (6) number of averaged individual data cubes, (7, 8) position angle θ in degrees and internal measurement error in tangential direction $\rho\sigma_\theta$ in mas, (9, 10) separation ρ in arcseconds and its internal error σ_ρ in mas, and (11) magnitude difference Δm. An asterisk follows if Δm and the true quadrant are determined from the resolved recentered image; a colon indicates that the data are noisy and Δm is likely overestimated (see TMH10 for details); the flag "q" means that the quadrant is determined from the SAA image (Section 2.4). Note that in the cases of multiple stars, the positions and photometry refer to the pairings between individual stars, not the photocenters of subsystems.

For binary stars with known orbital elements, Columns (12–14) of Table 3 list the residuals to the ephemeris position and code of reference to the orbit adopted in the Sixth Catalog of Orbits of Visual Binary Stars (Hartkopf et al. 2001, hereafter VB6).[8]

Table 4 contains the data on 426 unresolved stars, some of which are listed as binaries in WDS or resolved here in other filters. Columns (1) through (6) are the same as in Table 3,

---

[8] See http://ad.usno.navy.mil/wds/orb6/wdsref.html.

Table 3
Measurements of Double Stars at SOAR (Fragment)

WDS (2000)	Discoverer Designation	Other Name	Epoch +2000	Filt	N	θ (deg)	$\rho\sigma_\theta$ (mas)	ρ ($''$)	$\sigma\rho$ (mas)	Δm (mag)	$[O-C]_\theta$ (deg)	$[O-C]_\rho$ ($''$)	Reference Code[a]
00024+1047	A 1249 AB	HIP 190	17.6802	I	2	246.4	0.5	0.3003	0.1	0.8 q	−0.1	0.041	Zir2003
00029−7436	TDS 3 AB	CD−75 1309	17.6804	I	2	46.8	1.4	1.5189	0.5	0.6			
00036−3106	TOK 686	HIP 290	16.9487	I	3	13.3	0.8	0.1293	12.0	3.6			
			17.6801	I	2	24.1	10.0	0.1320	1.0	4.1			
00039−5750	I 700	HIP 306	16.9596	I	2	167.1	0.3	0.2557	0.1	0.3			
00061+0943	HDS 7	HIP 510	17.6802	I	2	196.3	0.3	0.2604	0.1	0.3	0.2	0.003	FMR2017c
00098−3347	SEE 3	HIP 794	17.6801	I	2	123.6	0.1	0.9069	0.1	1.0	1.9	0.007	Hrt2010a
00100+0835	A 1801	HIP 807	17.6802	I	2	198.5	0.1	0.3164	0.2	0.3			
00106−7313	I 43 AB	HIP 865	17.6011	I	3	196.0	0.7	0.4956	0.7	1.3	−0.6	−0.009	Cve2010e
00121−5832	RST 4739	HIP 975	16.9596	I	2	282.9	0.2	0.2853	0.1	0.2			
			17.6008	I	2	279.3	1.3	0.2776	0.5	0.0:			
00135−3650	HDS 32	HIP 1083	16.9487	I	2	11.4	0.5	0.2592	0.2	0.8 q	0.0	0.000	Tok2017b

Note.
[a] References to VB6 are provided at http://ad.usno.navy.mil/wds/orb6/wdsref.txt.

(This table is available in its entirety in machine-readable form.)

although Column (2) also includes other names for objects without discoverer designations. For stars that do not have entries in WDS, WDS-style codes based on the J2000 position are listed in Column (1). Column (7) is the estimated resolution limit, equal to the diffraction radius λ/D for good-quality data and larger for poor data (the effective resolution limit is computed from the maximum spatial frequency where the signal in the PS stands above the noise, see TMH10). Columns (8, 9) give the 5σ detection limits Δm at $0''.15$ and $1''$ separations determined by the procedure described in TMH10. When two or more data cubes are processed, the highest Δm value is listed. The last column marks with colons noisy data mostly associated with faint stars. In such cases, the quoted detection limits might be too large (optimistic); however, the information that these stars were observed and no companions were found is still useful. In a few instances, $\Delta m(0''.15) = 0$ indicates that the automatic procedure failed to determine a detection limit at close separation.

3.2. Most Tycho Binaries Are Spurious

The targets in run 4 featured all WDS binaries in the Kepler-2 fields, including those discovered by the *Tycho* mission (discoverer codes TDS and TDT). There are 17 targets with these codes in our data. One of them, TDT 721, is too wide to be resolved. Of the remaining 16, only one (TDT 3 at $1''.5$) is confirmed. The parameters of the *Tycho* pairs make them easily accessible to HRCam. We therefore conclude that a large number of *Tycho* binaries are spurious. Their supposed separations range from $0''.4$ to $3''$. Interestingly, we have resolved two more pairs in this group, but at different separations: WDS J16086−2540 at $1''.89$ and $\Delta I = 6.1$ mag (the TDS 9771 is listed with $0''.4$ separation and $\Delta m = 0.12$ mag) and WDS J17022−2820 at $0''.63$ and $\Delta I = 3.8$ mag (TDT 186 is listed at $0''.4$ and $\Delta m = 0.44$ mag). These faint companions are random discoveries unrelated to the previously claimed *Tycho* pairs.

The WDS contains 14,170 *Tycho* pairs; 330 of those have a code "X," i.e., are marked as spurious, while 1201 are confirmed. The veracity of most *Tycho* pairs still waits for confirmation.

3.3. Newly Resolved Pairs

Table 5 lists 44 newly resolved pairs. Its format is similar to that of Table 3. For some multiple systems, we used existing discoverer codes and simply added new component designations. The last two columns of Table 5 contain the spectral type (as given in SIMBAD) and the *Hipparcos* parallax p (van Leeuwen 2007). The *Gaia* (Gaia Collaboration et al. 2016) parallaxes, when available, are preferred; they are marked by asterisks. We comment on these objects below. The following abbreviations are used: PM—proper motion, CPM—common proper motion, RV—radial velocity, and SB1 and SB2—single- and double-lined spectroscopic binaries. Orbital periods are estimated from projected separation as

$$P^* = (\rho/p)^{3/2}M^{-1/2}, \qquad (1)$$

where ρ is the angular separation (assumed to equal the semimajor axis), p is the parallax, M is the mass sum, and P^* is the period in years. The statistical relation of these estimates to true periods is discussed by Tokovinin (2014). Data from the spectroscopic Geneva-Copenhagen Survey, GCS (Nordström et al. 2004), are used for some targets.

HIP 20802 (HD 28388) is a G6V astrometric binary (Makarov & Kaplan 2005), on the California exoplanet search program (Isaacson & Fischer 2010); Nidever et al. (2002) found an RV trend. Estimated period: 25 years.

HIP 35986 (HD 58249) has not been detected as an SB by the GCS, possibly owing to its fast axial rotation. Its small separation implies $P^* \sim 10$ years. The pair was not measured in run 5 because of the charge transfer problem, but was resolved again in 2017.3 (run 6) at similar PA and larger separation.

HIP 37012 (HD 45698) is a chemically peculiar Ap star resolved at $0''.14$, implying $P^* = 65$ years.

HIP 41800 (HD 72881) is a chemically peculiar Ap star without any prior hints on its binarity; $P^* = 30$ years. The six measures show a large scatter. However, without considering uncertain measures marked by colons, the position is stable over one year.

HIP 44914 (CD-37 5499) is a high-PM K5V dwarf star with only two references in SIMBAD. The new faint component at

Table 4
Unresolved Stars (Fragment)

WDS (2000) α, δ (J2000)	Discoverer Designation or Other Name	*Hipparcos* or Other Name	Epoch +2000	Filter	N	ρ_{min} (arcsec)	5σ Detection Limit		Δm Flag
							$\Delta m(0\rlap{.}''15)$ (mag)	$\Delta m(1'')$ (mag)	
00219−2300	RST 5493 A	HIP 1732	17.6801	I	2	0.041	2.53	5.68	
00291−0742	MLR 2	HIP 2275	17.6801	I	2	0.041	2.66	4.41	
00313−1909	B 6	HD 2797	17.6801	I	2	0.041	3.10	4.82	
00324+0657	MCA 1 Aa,Ab	HIP 2548	16.9595	I	2	0.040	2.93	4.61	
			16.9595	Hα	2	0.041	3.32	4.24	
			17.6802	I	2	0.041	2.22	4.56	
			17.6802	y	1	0.028	3.53	5.79	
			17.6802	Hα	1	0.039	3.73	5.01	
00366−4908	HIP 2888	HIP 2888	16.9596	I	2	0.040	4.13	6.21	
00374−3717	I 705	HIP 2944	16.9596	I	2	0.040	4.07	6.29	
			16.9596	y	2	0.028	4.39	6.05	
00467−0426	LSC 10 Aa,Ab	HIP 3645	16.9569	I	2	0.040	3.14	5.10	

(This table is available in its entirety in machine-readable form.)

$1\rlap{.}''34$ remained fixed in one year, hence it is physical. The period is long, $P^* = 900$ years.

HIP 52792 (HD 93527) has a CPM companion HIP 52793 at $30\rlap{.}''4$, which is itself an SB2 according to the GCS. The new close pair Aa,Ab is fast ($P^* = 2$ years), and we indeed see its fast retrograde motion in one year.

HIP 53938 (HD 95699, V360 Vel) is a chemically peculiar Ap star with periodic flux variability. The separation has slightly increased in one year, matching $P^* = 55$ years. There is a physical companion at $19\rlap{.}''2$.

HIP 54553 (BD+16 2222) is a nearby M0V dwarf GJ 9348 with a relatively fast PM. The new companion at $2\rlap{.}''6$ is confirmed as physical in 2018.

HIP 57600 (HD 102698) is another nearby K4V dwarf known as an astrometric (acceleration) binary (Makarov & Kaplan 2005). A fast retrograde motion of the new pair is seen, in agreement with $P^* = 5$ years. The wide companion TOK 281 with similar PM listed in WDS at $407''$ separation is likely optical.

HIP 57698 (HD 102804) is on the *Magellan* exoplanet search program. The newly found companion at $0\rlap{.}''60$ can cause a measurable RV trend despite its long $P^* = 350$ years. The pair is confirmed as physical by its reobservation in 2017.

HIP 58084 (BD-13 3470) is a K6V dwarf found here to be a $0\rlap{.}''07$ pair with nearly equal components and fast retrograde motion, in agreement with the estimated period $P^* = 10$ years.

HIP 62445 (HD 111170, V940 Cen) is a young chromospherically active G9IV star in the Sco-Cen association. The newly resolved pair has $P^* = 5$ years and shows some orbital motion in one year. The large discrepancy between the *Hipparcos* (7.7 mas) and *Gaia* DR1 (13.2 mas) parallaxes is presumably caused by the effect of orbital motion on the astrometric data reduction (the DR2 parallax is 7.9 mas).

HIP 62985 (ψ Vir, HR 4902) is a bright M-type giant with 149 references in SIMBAD. The faint binary companion detected in 1975 by lunar occultations (OCC 387 in the WDS) was directly resolved for the first time in 2016 at $0\rlap{.}''21$ and confirmed next year. The estimated period is ∼100 years.

HIP 63012 (HD 112145) is featured in the GCS, but otherwise it has attracted no interest so far. The new $0\rlap{.}''16$ pair

with $P^* = 80$ years is also not interesting because of its slow expected motion.

HIP 63377 (HD 112636) has a companion at $0\rlap{.}''42$. The resolution is very secure, but no second measure has been taken so far. Only a slow motion is expected, $P^* = 160$ years.

HIP 69113 (HD 123445) is a bright B9V member of the Sco-Cen association. It was pointed instead of the fainter pair DE, at $5\rlap{.}''3$ from the component A. Detection of the new 56 mas, nearly equal pair Aa,Ab is secure; it is confirmed in 2018, at closer separation. The estimated period is $P^* = 12$ years.

HIP 69549 (HD 124605) has a fast PM and an RV of -88.9 km s^{-1}; it is likely metal poor. Its resolution at $0\rlap{.}''08$ in 2016.14 is secure; however, the pair closed down and was unresolved in 2017.37; $P^* = 13$ years.

HIP 70693 (HD 126620) is a new $0\rlap{.}''05$ pair with $P^* = 8$ years. Its reobservation shows decreasing separation at nearly constant PA.

HIP 72492 (HD 130264) is the *Hipparcos* pair HDS 2092 revealed here as a new triple system; we resolve the secondary into a $0\rlap{.}''057$ pair BC and observe its direct motion; $P^*_{BC} = 20$ years. Like some other triple dwarfs (Tokovinin 2018c), this is a "double twin": the estimated masses of B and C are about $0.8\mathcal{M}_\odot$ each, and their sum is close to the mass of the main component A, $1.6\ \mathcal{M}_\odot$.

HIP 77843 (HD 142269) is a new $0\rlap{.}''13$ pair with a fast motion, $P^* = 21$ years.

HIP 78475 (HD 143235) is a $0\rlap{.}''7$ neglected binary SEE 254 observed as a "filler" to the main program. We discovered it to be a triple system where the primary component is a $0\rlap{.}''064$ pair. The separation implies $P^* \sim 12$ years (we do see some motion in one month). The orbit of the subsystem could be computed now from the wobble in the trajectory of the outer pair if accurate measurements were available. Unfortunately, this is not the case.

J16086-2540 (HD 144785) in the *K2* field is resolved at $1\rlap{.}''89$, $\Delta I = 6.1$ mag; the $0\rlap{.}''4$ *Tycho* pair TDS 1977 is spurious, see Section 3.2.

HIP 80925 (HD 148704), a nearby K1V star with fast PM, is a spectroscopic binary with $P = 31.8$ days. The newly resolved pair Aa,Ab has $P^* = 1.5$ years; it should be detectable by RV

Table 5
Newly Resolved Pairs

WDS (2000)	Discoverer Designation	Other Name	Epoch +2000	Filt	θ (deg)	ρ (″)	Δm (mag)	Spectral Type	p (mas)
02460−0457	BU 83 Aa,Ab	HIP 12912	16.9590	I	67.8	0.2231	4.3	F3V	13.2
04274−2912	TOK 709	HIP 20802	16.1373	I	68.7	0.1278	2.1 q	G6V	12.1*
06272−3706	TOK 710	HIP 30712	16.1330	I	159.4	0.1392	2.3 q	ApSrEu	6.0*
07250+0406	TOK 711	HIP 35986	16.1346	I	156.2	0.0301	0.7	G0V	6.7*
08314−6531	TOK 712	HIP 41800	16.1373	I	203.3	0.0517	1.1 q	ApSi	4.0
09090−3802	TOK 713	HIP 44914	16.1375	I	266.5	1.3401	2.0*	K5V	14.4*
10476−1538	TOK 714 Aa,Ab	HIP 52792	16.1376	I	72.9	0.0294	0.1	F7II/III	13.1*
11022−4230	TOK 715 Aa,Ab	HIP 53938	16.1376	I	125.0	0.1174	1.7 q	ApSrEuCr	5.2
11098+1531	TOK 716	HIP 54553	16.1351	I	248.0	2.6180	2.0*	M0V	23.0*
11495−1636	TOK 717 Aa,Ab	HIP 57660	16.1351	I	81.3	0.0682	0.5 q	K4V	19.0*
11500−5616	TOK 718	HIP 57698	16.1377	I	202.1	0.6002	3.2	F3V	8.4*
11547−1401	TOK 719	HIP 58084	16.1351	I	130.6	0.0732	0.3:	K6V	13.9*
12479−5127	TOK 720	HIP 62445	16.1353	I	176.1	0.0485	0.7	G9IVe	13.2*
12544−0932	OCC 387	HIP 62985	16.3890	y	111.7	0.2116	3.7	M2III	6.0
12547−3930	TOK 721	HIP 63012	16.1354	I	320.8	0.1647	2.9 q	F7V	6.7*
12592−6256	TOK 722	HIP 63377	16.1351	I	55.1	0.4176	2.4 q	G3V	11.2
14089−4328	HJ 4653 Aa,Ab	HIP 69113	17.2833	I	95.2	0.0555	0.1	B9V	6.2
14142+1805	TOK 723	HIP 69549	16.1382	I	350.6	0.0816	2.4	G0V	11.6*
14275−3527	TOK 724	HIP 70693	16.1354	I	138.5	0.0532	0.2	F8V	10.8
14494−5726	HDS 2092 BC	HIP 72492	16.1406	I	170.0	0.0567	0.3	F5V	8.2*
15537−0429	TOK 725	HIP 77843	16.1410	I	32.8	0.1270	1.3 q	F8/G0V	12.5
16012−4632	SEE 254 Aa,Ab	HIP 78485	17.4324	y	192.7	0.0637	1.3:	F6V	9.0
16086−2540	TOK 726	HD 144785	16.3876	I	63.7	1.8879	6.1*	G8IV	…
16315−3901	HDS 2335 Aa,Ab	HIP 80925	16.3907	I	68.6	0.0724	2.0	K1V	44.5*
16385+1240	TOK 727	HIP 81476	17.4327	I	176.4	0.0876	2.1	G0	10.2*
17022−2820	TOK 728	HD 153709	16.3876	I	164.4	0.6349	3.8:	A0IV/V	…
17086−2650	SEE 319 Aa,Ab	HIP 83878	16.3876	I	40.2	0.0422	0.9	B9IV	3.5
17095−2612	SKF 2521 Aa,Ab	CPD−26 5829	16.3876	I	161.0	0.1214	0.3:	F8	…
17379−3752	I 247 AC	HIP 86286	17.5345	I	350.5	0.1772	2.2	G8IV	21.0
18086−2752	BU 244 Ba,Bb	HIP 88864	16.3877	I	146.1	0.1238	1.9	G8III	3.5
19035−2645	LDS 5870 Aa,Ab	K214324736	16.3882	I	66.8	0.5227	3.9:	G5V?	9.4*
19139−2548	B 2475 Aa,Ab	HD 179499	16.3880	I	118.3	0.3894	1.7 q	F8	2.7*
19164−2521	HJ 5101 Aa,Ab	HD 180132	16.3880	I	127.1	0.6919	4.4	B9/A0V	2.8*
19197−2836	B 433 AC	HIP 94985	16.3880	I	51.7	2.4366	3.9	G1V	8.4
19231−2833	RSS 520 Aa,Ab	HIP 95278	16.3880	I	156.6	0.3490	2.8:	F0	1.3
19239−2939	HJ 5110 Aa,Ab	CD−29 16082	16.3880	I	215.8	0.1166	0.9:	F4V	1.2*
19391−2811	B 444 Aa,Ab	HD 185233	16.3880	I	27.3	0.1002	1.5:	A5III	…
20100−1303	TOK 729	HIP 99357	17.8246	I	277.2	1.2429	6.1*	F5V	4.4
21012−3511	TOK 344 Aa,Ab	HIP 103735	17.6025	I	168.0	0.1747	1.7	G3V	21.5
20212+0249	TOK 730	HIP 103735	16.3900	I	143.85	0.2269	2.3	G0	2.3
21266−4604	HJ 5267 Aa,Ab	HIP 105879	17.6027	I	53.6	0.0874	1.9	F7V	15.8
21278−5922	TOK 731	HIP 105976	16.3883	I	27.3	0.1002	1.5:	F2IV	8.0
21357−5942	TOK 732	HIP 106615	16.3901	I	185.3	0.7033	3.3 q	G0V	12.3
23005−3345	TOK 733	HIP 113598	17.8248	I	62.9	0.0634	1.4	G4V	12.3*

variation. On the other hand, the 4″ binary HDS 2335 is optical; the companion B is seen in 2MASS at 9.″4, 25.°9.

HIP 81476 (HD 150122) was known to be a binary from its variable RV and astrometric acceleration. It belongs to the 67 pc sample of nearby dwarfs, although the *Gaia* parallax of 10.2 mas now places it outside 67 pc. D. Latham (2012, private communication) computed an unpublished nine-year spectroscopic orbit. The star was observed at SOAR and unresolved in 2014.30, but now it is securely resolved at 0.″088 separation. With $\Delta I = 2.1$ mag, double lines should be detectable in the spectrum, opening the prospect of accurate mass measurement. The star is on the California program of planet search (Isaacson & Fischer 2010).

J17022−2820 (HD 153709) is a new pair with 0.″63 separation and $\Delta I = 3.8$ mag (below the estimated 5σ detection limit of 3.4 mag). It was observed as the *Tycho* binary TDT 186, which is revealed to be spurious, see Section 3.2.

HIP 83878 (SEE 319) is a B9IV star with a slow PM. The status of the known companion at 7.″7 is uncertain (it can be optical). The newly detected subsystem Aa,Ab at 0.″042, confirmed a year later, has an estimated period of ∼20 years.

CPD−26 5829 (SKF 2521) is another wide 7.″4 binary from the *K2* program where we found a subsystem Aa,Ab. With the photometric parallax of 3.2 mas, the estimated period of Aa,Ab is longer than 100 years; no motion is detected in 1 year.

HIP 86286 is the known visual binary I247. Unexpectedly, we found two companions B and C of similar brightness in a nearly equilateral configuration, both at 0.″2 separation from the primary. In 1897, the separation was 1″. It steadily decreased during the 20th century, in agreement with the long

estimated period $P^* = 200$ years. Presumably, the secondary component is a close binary BC that has not been recognized until now. This object resembles the similar equilateral triple I 213 discovered at SOAR in 2015 (Tokovinin et al. 2016b).

HIP 88864 (HD 165732) is a G8III giant. In addition to the known 2″2 pair BU 244, we measured the subsystem Ba,Bb at 0″12. Reobservation after one year revealed its retrograde motion, although the parallax of 3.5 mas implies $P^*_{Ba,Bb} = 120$ years.

EPIC 214324736 (TYC 6881-1560-1) is the 17″4 CPM pair LDS 5870 with the *Gaia* parallax of 9.4 mas. The components' PMs and photometric distances match. WDS lists a discordant first measure in 1960, which, if true, would mean that AB is optical; we believe the first measure to be in error because the configuration of AB remained fixed for 15 years between its measurements by 2MASS and *Gaia*. The newly discovered 0″52 subsystem Aa,Ab is also fixed, proving its physical nature; $P^*_{Aa,Ab} = 330$ years.

HD 179499 is the known visual pair B 2475 at 8″2 separation. The *Gaia* parallax of the secondary component is 2.7 mas, while it gives no parallax for the primary, possibly because it was resolved. Indeed, we discovered Aa,Ab at 0″39; its position did not change in a year. Its estimated orbital period is ∼1 kyr. However, the F8 spectral type of A and the colors of both A and B indicate a photometric parallax of 5 mas, inconsistent with the *Gaia* parallax.

HD 180132 is a 21″4 pair HJ 5101 AB. Matching *Gaia* parallaxes and PMs of both components leave no doubt that this pair is physical, despite its first discordant measure in WDS. The companion to A discovered here at 0″69 is probably too faint to be detected by *Gaia* ($\Delta I = 4.4$ mag). The period of Aa,Ab is long, ∼2 kyr; its position is fixed during one year.

HIP 94985 is a tight 0″2 binary B433 to which we discovered a faint ($\Delta I = 3.9$ mag) companion at 2″44. If the companion were a distant unrelated star with a zero PM, the separation of AC would have increased by 38 mas in one year. Instead, we found it to be constant to within 3 mas. The 0°4 change in the PA during this period is likely related to the angle calibration problems in run 3.

HIP 95278 is a 9″7 pair RSS 520 located in a relatively crowded region of the sky; its faint secondary component is likely optical. The small PM and parallax do not help in defining its status. The newly discovered subsystem Aa,Ab at 0″39 has a better chance to be physical, but its long period of ∼2.5 kyr does not inspire any interest in this discovery.

CD−29 16082 (HJ 5110) is a 5″9 near-equal pair where we found a 0″12 subsystem Aa,Ab. This triple system could be physical. However, the *Gaia* parallax of 1.2 mas implies very long periods; if the parallax is correct, both components A and B are located above the main sequence.

HD 185233 is a 1″ binary B444 without trigonometric parallax or orbit. We discovered the 0″10 subsystem Aa,Ab. This resolution, although not checked in 2017, is secure. The expected period of Aa,Ab is several centuries, given the photometric parallax of 1.9 mas.

HIP 99357 (HD 191365) is an F5V spectroscopic binary according to the GCS, based on two mutually discordant measures of the RV. The new faint companion at 1″34 with $\Delta I = 6.1$ mag may be optical.

HIP 100355 was pointed in 2015 by mistake instead of HLD 158 (WDS J20213+0250) and resolved at 0″2, in marked disagreement with the orbit of HLD 158 (Tokovinin

et al. 2016b). Now the confusion is clarified, as both HIP 100355 and HLD 158 were measured. Our published 2015 measure should be attributed to HIP 100355.

HIP 103735 (HD 199918) is a nearby G3V star with a wide (186″) CPM companion, which possibly is a white dwarf. The main star is a spectroscopic and astrometric binary, first resolved here at 0″17. The separation implies an orbital period on the order of 20 years that might explain the non-resolution of this binary at Gemini in 2011 (Tokovinin et al. 2012).

HIP 105879 (HD 203934) has astrometric acceleration and variable RV (CGS). Its spectrum has double lines, according to the ongoing monitoring at the CTIO 1.5 m telescope. The first attempts to resolve the pair at Gemini (Tokovinin et al. 2013) and at SOAR in 2015.74 were unsuccessful, but in 2017.6, it was securely resolved at 0″087. The separation and magnitude difference match the preliminary spectroscopic orbit with $P = 5$ years and the mass ratio $q = 0.78$. According to this orbit, the separation in 2015.74 was 0″025. Observations for several more years will lead to accurate measurements of the masses of components Aa and Ab; the next periastron is predicted in 2020.6. The CPM companion D at 44″ makes this system triple. Star D has a constant RV, and it has not been resolved at SOAR in 2014.

HIP 105976 (HD 203970) is resolved at 0″09 in 2016.4; it moved by 8° in one year, matching the estimated period $P^* = 30$ years.

HIP 106615 (HD 205158) has a new faint companion at 0″70 with $P^* = 300$ years. The star is on the *Magellan* planet search program.

HIP 113598 (HD 217344) is a 3″9 physical pair B 582 containing a 1.6 day SB1 TZ PsA. We tentatively resolved an intermediate subsystem Aa,Ab at 0″063. However, this result needs confirmation because telescope vibrations could mimic the resolution. If this pair is real, its period is short, $P^* = 8$ years.

3.4. The Triple System BU 83

One of the calibrator binaries, WDS J02460−0457 (BU 83, HIP 12912, ADS 2111, F3V), is found to be triple. Looking back at the archival SOAR data, the tertiary component can be noted in several *I*-band ACFs. The clearest previous detection was in 2012.92, but it was overlooked at the time. The inner pair Aa,Ab was then at 58°7, 0″20, $\Delta I = 4.5$ mag; it turned by 23° in five years. A very tentative measure of Aa,Ab in 2009.671 is 58°9, 0″19. In 2015, the companion's detection was marginal, but it was resolved securely in 2016 and 2017 (Figure 4). The companion is not seen in the *y* band. Owing to the faintness of the companion Ab, the fitted triple-star models do not converge well, resulting in the low accuracy of the measures of Aa,Ab.

Interestingly, the existence of the subsystem was suspected by Dommanget (1972) from the run of the residuals of the outer pair. He proposed a 36-year astrometric orbit with an amplitude of 0″08.

Figure 5 shows that the accurate SOAR measures indeed deviate from the long-period orbit (which itself is poorly defined by the short observed arc). Using the orbit3.pro code[9] (Tokovinin & Latham 2017), we can fit the wobble and the resolved measures of Aa,Ab by two sets of orbital elements. However, the low accuracy of historic measures and the partial coverage of the inner resolved orbit make such fits rather
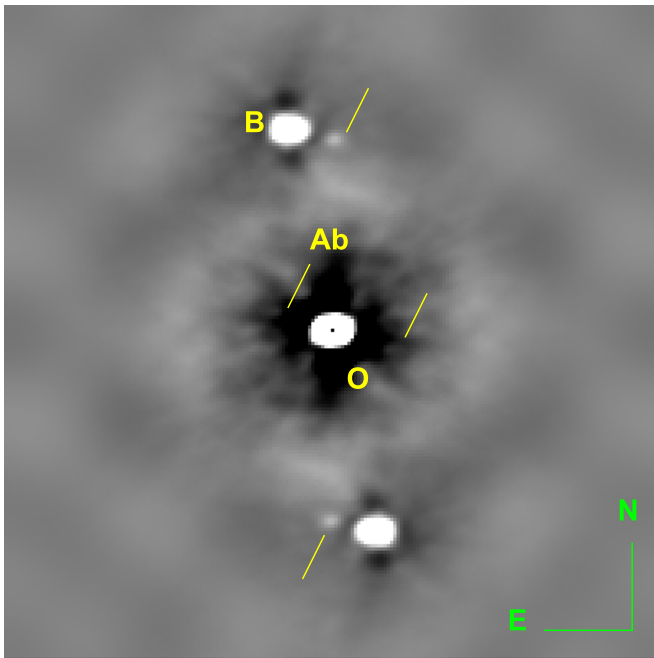
---

9 10.5281/zenodo.321854

Figure 4. ACF of BU 83 recorded on 2017.83 in the *I* band. The coordinate center is at O, the letters indicate the two peaks corresponding to B and Ab, while lines mark all four peaks caused by the faint component Ab (the two central peaks are lost in the noise).
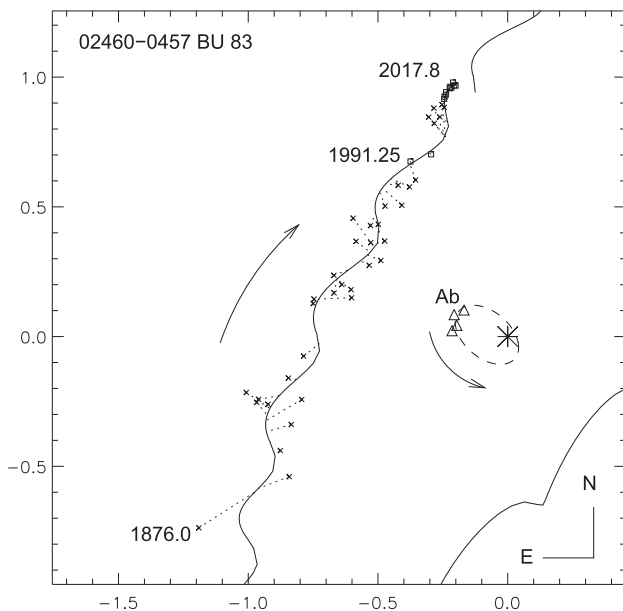

Figure 5. Trajectory of the outer subsystem in BU 83 accounting for the wobble caused by the inner subsystem. Crosses indicate micrometer measures and speckle interferometry at small apertures, squares show accurate recent measures at SOAR and *Hipparcos*, and line depicts the orbit. The dashed ellipse and triangles denote the orbit and resolved measures of the subsystem Aa,Ab. The axis scale is in arcseconds.

uncertain. The plots in the figure correspond to an inner period of 38 years and an outer period of 915 years. The inner subsystem has direct motion, while the outer orbit is retrograde, so the angle between the inner and outer angular momentum vectors is large. The sign of the wobble confirms that the

subsystem belongs to the primary component. Patient accumulation of measures is needed before attempting a meaningful analysis of this interesting triple system. The intuition of J. Dommanget, who discovered the wobble in the noisy measures available prior to 1972, is truly amazing, but the astrometric orbit derived from the old data alone cannot be trusted.

ORCID iDs

Andrei Tokovinin ⓘ https://orcid.org/0000-0002-2084-0782
William I. Hartkopf ⓘ https://orcid.org/0000-0001-6111-4560
Elliott P. Horch ⓘ https://orcid.org/0000-0003-2159-1463

References

Briceño, C., & Tokovinin, A. 2017, AJ, 154, 195
Dommanget, J. 1972, Bull. RAS Belg., 8, 63
Gaia Collaboration, Brown, A. G. A., Vallenari, A., Prusti, T., et al. 2016, A&A, 595, 2
Gomez, J., Docobo, J. A., Campo, P. P., & Mendez, R. 2016, AJ, 152, 216
Hartkopf, W. I., Mason, B. D., & Worley, C. E. 2001, AJ, 122, 3472
Hartkopf, W. I., Tokovinin, A., & Mason, B. D. 2012, AJ, 143, 42
Horch, E. P., Casetti-Dinescu, D. I., Camarata, M. A., et al. 2017, AJ, 153, 212
Horch, E. P., van Belle, G. T., Davidson, J. W., Jr., et al. 2015, AJ, 150, 151
Isaacson, H., & Fischer, D. 2010, ApJ, 725, 875
Makarov, V. V., & Kaplan, G. H. 2005, AJ, 129, 2420
Mason, B. D., Hartkopf, W. I., Miles, K. N., et al. 2018, AJ, in press, arXiv:1804.07845
Mason, B. D., Wycoff, G. L., Hartkopf, W. I., et al. 2001, AJ, 122, 3466, (WDS)
Mendez, R. A., Claveria, R. M., Orchard, M. E., & Silva, J. F. 2017, AJ, 154, 187
Muterspaugh, M. W., Fekel, F. C., Lane, B. F., et al. 2010a, AJ, 140, 1646
Muterspaugh, M. W., Hartkopf, W. I., Lane, B. F., et al. 2010b, AJ, 140, 1623
Nidever, D. L., Marcy, G. W., Butler, R. P., et al. 2002, ApJS, 141, 503
Nordström, B., Mayor, M., Andersen, J., et al. 2004, A&A, 418, 989, (GCS)
Sauvage, J.-F., Fusco, T., Guesalaga, A., et al. 2015, in Proc. Conf., Adaptive Optics for Extremely Large Telescopes 4, http://www.escholarship.org/uc/item/910646qf
Tokovinin, A. 2012, AJ, 144, 56
Tokovinin, A. 2014, AJ, 147, 86
Tokovinin, A. 2016, AJ, 152, 138
Tokovinin, A. 2017, AJ, 154, 110
Tokovinin, A. 2018a, PASP, 130, 5002
Tokovinin, A. 2018b, Inf. Circ., 194, 1
Tokovinin, A. 2018c, AJ, 155, 160

Tokovinin, A., & Cantarutti, R. 2008, PASP, 120, 170
Tokovinin, A., Cantarutti, R., Tighe, R., et al. 2010a, PASP, 122, 1483
Tokovinin, A., Cantarutti, R., Tighe, R., et al. 2016a, PASP, 128, 125003
Tokovinin, A., Hartung, M., Hayward, Th. L., & Makarov, V. V. 2012, AJ,
    144, 7
Tokovinin, A., Hartung, M., & Hayward, T. L. 2013, AJ, 146, 8
Tokovinin, A., & Latham, D. W. 2017, ApJ, 838, 54

Tokovinin, A., Mason, B. D., & Hartkopf, W. I. 2010b, AJ, 139, 743,
    (TMH10)
Tokovinin, A., Mason, B. D., & Hartkopf, W. I. 2014, AJ, 147, 123
Tokovinin, A., Mason, B. D., Hartkopf, W. I., et al. 2015, AJ, 150, 50,
    (SOAR14)
Tokovinin, A., Mason, B. D., Hartkopf, W. I., et al. 2016b, AJ, 152, 116
van Leeuwen, F. 2007, A&A, 474, 653